

Difference melt model

Saule Sh. KAZHIKENOVA, Sagyndyk N. SHALTAKOV and Bekbolat R. NUSSUPBEKOV

The basic objective of the research is to construct a difference model of the melt motion. The existence of a solution to the problem is proven in the paper. It is also proven the convergence of the difference problem solution to the original problem solution of the melt motion. The Rothe method is implemented to study the Navier–Stokes equations, which provides the study of the boundary value problems correctness for a viscous incompressible flow both numerically and analytically.

Key words: Navier–Stokes equations, hydrodynamic, approximations, mathematical models, melt

1. Introduction

It is impossible to model numerically the melt motion without taking into account the mathematical aspects of solving the equations of hydrodynamics. To describe the motion of melts in this work, we consider the continuity equation and the Navier–Stokes equations, which are a consequence of the mass and momentum conservation application to the elementary volume of a liquid.

The theory of Navier–Stokes equations is well established in its content and development, therefore it sets increasingly more new mathematical problems related not only to applications in hydrodynamics, but also in such fundamental mathematics areas as the theory of functional spaces embedding, potential theory, interpolation theory and so on. This theory allows to solve many problems related to the molten state and has a positive impact on the liquid state physics progress, the theory of metallurgical processes and in turn metallurgical technologies.

Copyright © 2021. The Author(s). This is an open-access article distributed under the terms of the Creative Commons Attribution-NonCommercial-NoDerivatives License (CC BY-NC-ND 4.0 <https://creativecommons.org/licenses/by-nc-nd/4.0/>), which permits use, distribution, and reproduction in any medium, provided that the article is properly cited, the use is non-commercial, and no modifications or adaptations are made

S.Sh. Kazhikenova (corresponding author, e-mail: sauleshka555@mail.ru, ORCID: 0000-0002-6937-1577) and S.N. Shaltakov (ORCID: 0000-0002-1186-1178) are with Karaganda Technical University, Kazakhstan.

B.R. Nussupbekov Bekbolat (ORCID: 0000-0003-2907-3900) is with the Karaganda University E.A. Buketov, Kazakhstan.

Received 09.04.2021. Revised 19.08.2021.

Section 2 of the paper presents the problem formulation and relation to the literature. Navier–Stokes equations in the form corresponding to the certain melt motion aspects are introduced in Sec. 3, where the main results of the research are presented, i.e. using of Rothe method for Navier–Stokes equations. We consider the copper melt flow in an inclined chute and interpret numerical modeling melt flow in Sec. 4. The theoretically determined optimum flow temperature of copper melt is consistent with the practical one, being in the optimum 1423–1558 [K] interval, which is close to the temperatures of real melt flow in industrial conditions. Sec. 5 of the paper presents the conclusion. The validity and reliability of theoretical studies have been confirmed by comparing the results with the parameters of the flow of copper melt in the technological equipment of Southwier–2000 line.

2. Problem formulation

Many systems of partial differential equations, linear and nonlinear, are used to describe physical phenomena. In this paper we have chosen to describe the Navier–Stokes equations which govern the flow of a viscous fluid. The Navier–Stokes equations are of primary importance in fluid mechanics, and exhibit by themselves all the main features and difficulties of nonlinear equations. There are several reasons why the study of the Navier–Stokes has been central in the activities of mathematicians for more than two centuries. The Navier–Stokes equations are perfectly well defined mathematical objects and are paradigms of nonlinear equations. The solutions exhibit in their behavior many characteristics of genuinely nonlinear phenomena.

In view of the needs of practical applications in engineering sciences success has been limited. It is known that the Navier–Stokes equations are analytically unsolvable in general. Analytical solutions have been reported only for relatively trivial cases [1–4]. Therefore, our attention focuses on the numerical methods.

The present problems are: how can one describe the phenomena with adequate equations, how can one compute them, and visualize the results in spite of their complexity. The equations involve some physical parameters and turn out to be relevant when these parameters have certain values. Therefore as an introduction it is natural to consider a “chain” of equations, hoping, as is often the case, that the next equation will become relevant when the structure of the phenomena becomes too complicated to be computed by the previous one. The Navier–Stokes equations appear to be one of the main links in this chain [3]:

I Hamiltonian system of particles → II Boltzmann equation → III Navier–Stokes equations → IV Models of turbulence.

Each step is deduced from the previous one with the introduction of hierarchy of equations and a process of closure which in some cases leads to the appearance of irreversibility.

The development of numerical models of the equations of hydrodynamics is devoted to many scientific articles. Shortened version of the Navier–Stokes equations with viscous members are given in [4]. Correctness of the Cauchy problem formulation has been proved mathematically and general problems of the considered systems classification has been studied.

Further development of the problem is described in [5]. Solving method of three-dimensional hydrodynamic equations is based on the introduction of artificial compressibility. System of equations is solved by using an implicit scheme. It is proved that the method is fast converging.

An algorithm for solving the hydrodynamic equations in the three-dimensional curvilinear coordinates is presented in the works [6–8]. There are considered stationary and non-stationary flows of incompressible liquid.

Other methods are being sought. There is an attempt to derive the Navier–Stokes equation by using the variational method, as presented in [9]. Variational method is based on the natural decrease of the flow exergy. Author deals with the liquids thermodynamic properties.

We discuss the implementation of a numerical algorithm for simulating incompressible fluid flows. A first we have to investigate Rothe’s scheme for the Navier–Stokes equations in two dimensional bounded domains with slip boundary conditions admitting flow across the boundary. The structure of the model enables to reformulate it into the coupled system of the vorticity and velocity problems. The method is based on the maximum principle for the vorticity equation which delivers a new bound for the solutions.

3. Nonlinear Navier–Stokes equations

The main objective of this study is the melt motion description, assumed that there are known the external forces acting on the melt in the boundary mode and, the initial velocity field for a non-stationary flow. Basically, we assume that there is a coordinate system in which the field with the melt are unchanged. The assumption of the field constancy is fulfilled in such practically important tasks as the problem of the solid body flowing with an infinite flow; the problem of the liquid motion under the action of volume forces in a vessel and others.

Consider a mathematical model of a melt in melting bath:

$$\frac{\partial v}{\partial t} + (v \cdot \nabla)v = \mu_0 \frac{\partial^2 v}{\partial x_3^2} + \mu \Delta v - \nabla \xi + f(\theta), \quad (1)$$

$$\frac{\partial \xi}{\partial t} + \int_0^H \operatorname{div} v \, dx_3 = 0, \quad (2)$$

$$\frac{\partial \theta}{\partial t} + (v \cdot \nabla) \theta = \lambda \frac{\partial^2 \theta}{\partial x_3^2} + \lambda \Delta \theta, \quad (3)$$

with initial boundary conditions:

$$\begin{aligned} v|_{t=0} = v_0(x), \quad \xi|_{t=0} = \xi_0(x), \quad \theta|_{t=0} = \theta_0(x), \\ t \in [0, T], \quad v|_S = 0, \quad \theta|_S = 0, \end{aligned} \quad (4)$$

where v – velocity, θ – temperature, ξ – surface level.

Here:

$$v = \left(v_1, v_2, - \int_0^{x_3} \operatorname{div} v \, dx_3 \right), \quad \operatorname{div} v = \frac{\partial v_1}{\partial x_1} + \frac{\partial v_2}{\partial x_2}, \quad \nabla \xi = \left(\frac{\partial \xi}{\partial x_1}, \frac{\partial \xi}{\partial x_2} \right),$$

where $f(\theta)$ – linear function of its argument.

For simplicity, assume: the area Ω is a cube, $\rho^\varepsilon \rightarrow \rho$ is border area of Ω .

We use the Rothe method [10, 11] for the problem (1)–(4). The Rothe method is being used to prove existence theorems and the actual definition of initial boundary value problems' solutions, the essence of which is in reducing these problems to boundary-value problems of elliptic type.

We conduct a discretization by time:

$$\frac{v^{n+1} - v^n}{\tau} + (v^n \cdot \nabla) v^{n+1} = \mu_0 \frac{\partial^2 v^{n+1}}{\partial x_3^2} + \mu \Delta v^{n+1} + f(\theta^n) - \nabla \xi^{n+1}, \quad (5)$$

$$\frac{\xi^{n+1} - \xi^n}{\tau} + \int_0^H \operatorname{div} v^{n+1} \, dx_3 = 0, \quad (6)$$

$$\frac{\theta^{n+1} - \theta^n}{\tau} + (v^n \cdot \nabla) \theta^{n+1} = \lambda_0 \frac{\partial^2 \theta^{n+1}}{\partial x_3^2} + \lambda \Delta \theta^{n+1}. \quad (7)$$

Equations (5)–(7) are solved with the following conditions:

$$\begin{aligned} \theta^0 = \theta_0(x), \quad v^0 = v_0(x), \quad \xi^0 = \xi_0(x), \\ \theta^{n+1}|_S = 0, \quad v^{n+1}|_S = 0, \quad 0 \leq n\tau \leq T < \infty. \end{aligned} \quad (8)$$

Lemma 1 Let $\theta_0(x) \in L_\infty(\Omega)$, $v_0(x) \in L_2(\Omega)$, $\xi_0 \in L_2(\Omega)$. Then in order to solve the problem (5)–(8) the following assessment is true:

$$\max_{0 \leq n\tau \leq T} \|v^n\| + \sum_{m=1}^N \tau \|\nabla v^m\|^2 \leq c < \infty,$$

$$\max_{0 \leq n \tau \leq T} \|\theta^n\|_{L^\infty(\Omega)} + \sum_{m=1}^N \tau \|\nabla \theta^m\|^2 \leq c < \infty.$$

Proof. By multiplying equation (7) by $(\theta^{n+1})^{2k+1}$, integrating by parts and discarding positive terms, we get the assessment:

$$\|\theta^n\|_{L^{2k}(\Omega)}^{2k} \leq \|\theta^0\|_{L^{2k}(\Omega)}^{2k}. \tag{9}$$

By assuming the application of the limit at $k \rightarrow \infty$, we have:

$$\|\theta^n\|_{L^\infty(\Omega)} \leq \|\theta^0\|_{L^\infty(\Omega)}.$$

Now let multiply the equation (7) by $2\tau\theta^{n+1}$, then it integrate over the area Ω . Therefore, we get:

$$\begin{aligned} & \|\theta^{n+1}\|^2 - \|\theta^n\|^2 + \|\theta^{n+1} - \theta^n\|^2 \\ & + 2\tau \int_{\Omega} (v^n \cdot \nabla) \theta^{n+1} \cdot \theta^{n+1} dx + 2\tau \left(\lambda_0 \left\| \frac{\partial \theta^{n+1}}{\partial x_3} \right\|^2 + \lambda \|\nabla \theta^{n+1}\|^2 \right) = 0. \end{aligned} \tag{10}$$

It can be noticed that:

$$\int_{\Omega} (v^n \cdot \nabla) \theta^{n+1} \cdot \theta^{n+1} dx = 0. \tag{11}$$

By taking into account the (11) equality from (10) we conclude:

$$\tau \sum_{n=0}^N \left(\lambda_0 \left\| \frac{\partial \theta^{n+1}}{\partial x_2} \right\|^2 + \lambda \|\nabla \theta^{n+1}\|^2 \right) \leq c < \infty.$$

Let multiply the equation (5) by $2\tau v^{n+1}$, and the equation (6) by $2\tau \xi^{n+1}$ and integrate the results by parts. Subsequently, we get the following:

$$\begin{aligned} & \|v^{n+1}\|^2 - \|v^n\|^2 + \|v^{n+1} - v^n\|^2 + 2\tau \int_{\Omega} (v^n \cdot \nabla) v^{n+1} \cdot v^{n+1} dx \\ & + \left[\mu_0 \left\| \frac{\partial v^{n+1}}{\partial x_3} \right\|^2 + \mu \|\nabla v^{n+1}\|^2 + (\nabla \xi^{n+1}, v^{n+1}) \right] \cdot 2\tau \\ & = 2\tau \int_{\Omega} f(\theta^n) \cdot v^{n+1} dx, \end{aligned} \tag{12}$$

$$\|\xi^{n+1}\|^2 - \|\xi^n\|^2 + \|\xi^{n+1} - \xi^n\|^2 + 2\tau \int_{\Omega} \int_{\Omega}^H \operatorname{div} v^{n+1} \cdot \xi^{n+1} dx_3 dx = 0. \quad (13)$$

By adding the equalities (12) and (13), after uncomplicated transformations we get:

$$\max_{0 \leq m\tau \leq T} (\|\xi^m\|^2 + \|v^m\|^2) + \sum_{m=1}^N \|\nabla v^m\|^2 \tau \leq c < \infty.$$

Thus, the Lemma is proved. \square

The following is true.

Theorem 1 *Let problem solution (1)–(4) be sufficiently smooth. Then difference problem solution (5)–(8) converges to the problem solution (1)–(4) with a velocity:*

$$\max_0 \leq n \leq N \|v^n - v(n\tau)\| + \tau \sum_{m=1}^N \|\nabla v^m - \nabla(v(m\tau))\|^2 \leq c(\tau)^2,$$

where $v(n\tau)$ – function value at the point (τ, x) .

Proof. Reserve of smoothness provides a compact set $\{v^n\}$ at $v(x, t)$ – less than some δ , determined by initial data and the existence of a limit vector-function $v(n\tau) \in L_2(\Omega)$, being the limit v^n at $\tau \rightarrow 0$. If substituted v^n into equations of system (1)–(3) and initial conditions (4), then the equations will be satisfied up to the right-hand sides, which tends to zero weakly. It follows that $v(n\tau)$ is a solution to the problem (1)–(4) and, due to the uniqueness of the problem solution (5)–(8) on the basis of the Lemma and embedding inequalities, it follows that v^n converges to $v(n\tau)$ at $\tau \rightarrow 0$ with velocity:

$$\max_{0 \leq n \leq N} \|v^n - v(n\tau)\| + \tau \sum_{m=1}^N \|\nabla v^m - \nabla(v(m\tau))\|^2 \leq c(\tau)^2.$$

The theorem is proved. \square

Theoretical hydrodynamics has long attracted attention of various specialties' scientists: comparative simplicity of the basic equations, precise problems formulation and clarity of its experiments inspired hope of getting a dynamic phenomena complete description occurring in melts [12–14].

4. The copper melt flow numerical modeling in an inclined chute

Let us consider melt flow in an inclined chute. For a particular design, one can interpret and consider it as follows. Direct axis Oz by chute axis, assuming that chute design is infinite, and the melt flow is directed along chute axis so that from

the three velocity components u , v , w , there is left only one w , therefore $u = 0$, $v = 0$. Let melt flow be isothermal, then density ρ and viscosity coefficient μ are constant.

Hence, the Navier–Stokes equations are given in the form:

$$\begin{aligned} -\frac{1}{\rho} \frac{\partial p}{\partial x} &= 0, \\ -\frac{1}{\rho} \frac{\partial p}{\partial y} &= 0, \\ w \frac{\partial w}{\partial z} &= -\frac{1}{\rho} \frac{\partial p}{\partial z} + \gamma \left(\frac{\partial^2 w}{\partial x^2} + \frac{\partial^2 w}{\partial y^2} + \frac{\partial^2 w}{\partial z^2} \right), \\ \frac{\partial w}{\partial z} &= 0. \end{aligned} \tag{14}$$

Thus, as can be seen from the system of equations (14), velocity w represents a function of only x , y coordinates besides that, the pressure function p is a function of coordinate z . The pressure changes narrowly from section to section, keeping the same value in the given section. Such movements are called established.

Based on (14) we obtain the following equation:

$$\frac{dp}{dz} = \mu \left(\frac{\partial^2 w}{\partial x^2} + \frac{\partial^2 w}{\partial y^2} \right). \tag{15}$$

The right hand side of (15) represents a function of x , y coordinates, then the left hand side is a function of z coordinate. The main statements follow from the hydrodynamics:

$$\frac{dp}{dz} = -\frac{\Delta p}{\ell},$$

where Δp is the pressure dropping in an arbitrarily selected area, ℓ is the chute length.

Besides that, due to the melt free surface presence in the chute, the pressure is equal to atmospheric one. Since chute is inclined to the horizon at a certain angle α , then a volume force arises, a projection of which onto the axis Oz is equal to $F_z = g \sin \alpha = \frac{\Delta p}{\ell}$. Then the motion equation (15) in the direction of Oz takes the form:

$$\mu \left(\frac{\partial^2 w}{\partial x^2} + \frac{\partial^2 w}{\partial y^2} \right) + \rho g \sin \alpha = 0. \tag{16}$$

Boundary conditions are necessary to be defined in order to solve obtained equation. These conditions will be determined by melt sticking to the chute bottom

and the friction absence on the melt free surface. Let us denote the flow depth as h_1 , and the width as h_2 . Then the problem boundary conditions are represented as follows:

$$\begin{aligned} w &= 0 & \text{at } y &= 0, \\ \frac{\partial w}{\partial y} &= 0 & \text{at } y &= h_1, \\ \frac{\partial w}{\partial x} &= 0 & \text{at } x &= h_2. \end{aligned} \quad (17)$$

Thus, the equation (16) with the boundary conditions (17) describe the melt flow process in concrete designs of chute type. The model is built for melting equipment of the SCR–2000 line, a sketch of which is presented in Fig. 1.

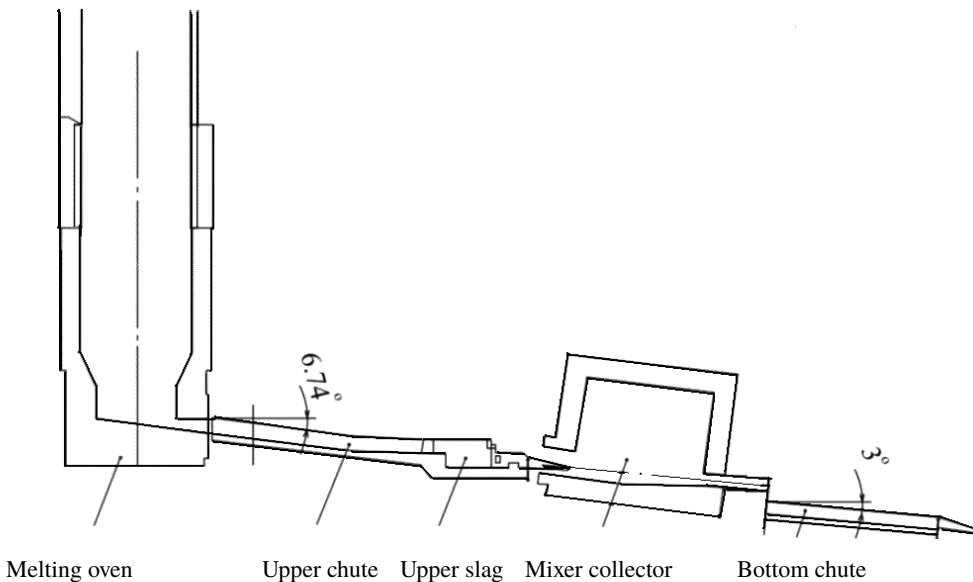


Figure 1: Sketch of the melting equipment SCR – 2000 line location

Calculations are made for the lower chute with an inclination angle of 3° as shown in Fig. 1. Cross section of the lower chute is presented in Fig. 2 where the melt level is depicted as well. Numerical parameters are determined by following calculations: the segment area is

$$S = \frac{[lr - a(r - h)]}{2},$$

where l – arc length, a – chord, h – segment arrow:

$$a = 83 \text{ [mm]}, \quad h = 18 \text{ [mm]},$$

$$l \approx \sqrt{a^2 + (16h^2/3)} = \sqrt{83^2 + (16 \cdot 18^2/3)} = 92.8 \text{ [mm]}.$$

$$\text{Hence } S = \frac{\left[92.8 \cdot \frac{115}{2} - 83 \left(\frac{115}{2} - 18 \right) \right]}{2} = 1029 \text{ [mm}^2\text{]}.$$

Then the second melt flow velocity is $Q = 3.61 \left[\frac{\text{kg}}{\text{s}} \right]$. With this taken into account it is possible to determine average melt flow velocity, which is equal to $v_{cp} = 0.45 \left[\frac{\text{m}}{\text{s}} \right]$. There were used a constant step sizes $\Delta x = \Delta y = 0.02$ in the calculations. Time step in the calculations was chosen to be equal to $\Delta t = 0.001$.

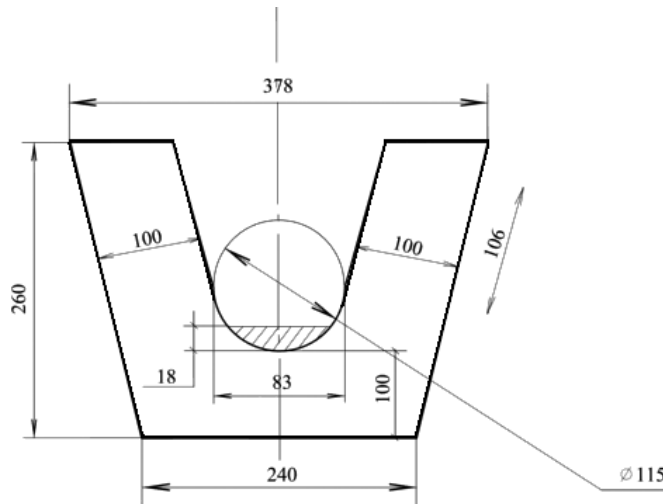


Figure 2: Section of lower chute (measurements given in [mm])

Established results for the velocities profiles v and u of melt flow profiles in the flat channel are presented in Fig. 3. Obtained results show that proposed computational scheme is efficient and can be used for calculating of the flow at sufficiently small Reynolds numbers without special difficulties.

Copper melt atoms at the moment of collisions approach as close as possible and are under the electrical forces action. In the time interval between thermal collisions, the copper melt atoms are rearranged in mutual location, jump in the force direction, and the atoms thermal movement occurs. When the melt flows in chute, no mixing of the melt various layers occurs, thus the copper melt flow can be represented as separate layers that move at different velocities, increasing towards melt surface. From the moment of atoms hopping in direction of the bulk force action, the flow is separated into the bottom layer and the main layer [9]. Bottom layer atoms are held at the bottom surface by the forces of interatomic

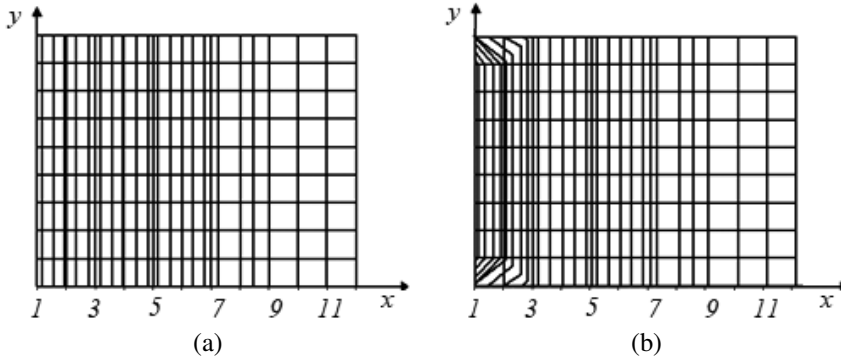


Figure 3: Profiles a) transverse v and b) longitudinal u velocities

adhesion with the surface, the main layer atoms under the bulk force action move along the bottom layer boundary. Chute walls, due to internal friction, inhibit the movement of the closest to it copper melt layer, and this inhibiting is transferred from one layer to another throughout the melt flow to the surface, where the flow is the fastest.

Taking into account the copper melt shear and bulk viscosities, the flow velocities distribution in the lower chute at a temperatures of 1358 [K], 1398 [K], 1438 [K], 1478 [K], 1518 [K], 1558 [K], 1598 [K], 1638 [K] in projections onto the XOY and also in XYZ spaces are presented in correspondence on Figs. 4–11 and Tables 1–8. It can be seen that the constant velocity lines, isolines, vary from $0.64 \left[\frac{m}{s} \right]$ to $0.01 \left[\frac{m}{s} \right]$. Moreover, the maximum flow velocity is achieved on surface, and at the chute bottom it is almost equal to zero, that is, completely consistent with the equations (14) and (15). Average value of velocity isoline is approximately equal to melt flow average velocity $v \approx 0.40 \left[\frac{m}{s} \right]$. Number of isolines at appropriate temperatures is as follows:

T [K]	1358	1398	1438	1478	1518	1558	1598	1638
n is number of isolines	19	21	23	24	26	28	12	12

These data show that the number of isolines passes through a maximum at a temperature of 1558 [K]. At lower temperatures, for example, at 1358 [K], and also at high temperatures, for example, at 1598 [K], velocity distribution is not so dense. This is probably due to the fact that the melt near the melting point is nonhomogeneous due to the formation clusters existence in it. And nonhomogeneity at temperatures of 1598 [K] and higher is associated with thermal loosening of molten metal structure and is not technologically feasible, since it leads to mechanical defects while the final product is formatted.

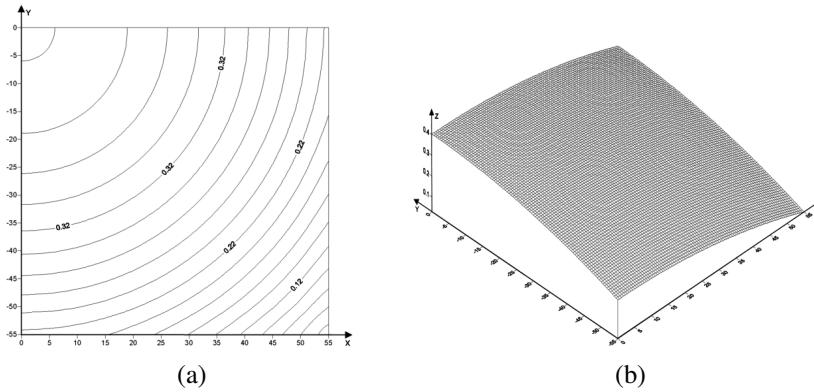


Figure 4: Velocity isolines a) and surface b) at a temperature of 1358 [K]

Table 1. Copper melt's flow velocity profiles at temperature of 1358 [K]

Y	X					
	0.0000	5.0000	10.000	15.000	20.000	25.000
0.0000	0.4023	0.4007	0.3961	0.3883	0.3775	0.3636
-5.00	0.4007	0.3992	0.3945	0.3868	0.3760	0.3620
-10.00	0.3961	0.3945	0.3899	0.3821	0.3713	0.3574
-15.00	0.3883	0.3868	0.3821	0.3744	0.3636	0.3496
-20.00	0.3775	0.3760	0.3713	0.3636	0.3527	0.3388
-25.00	0.3636	0.3620	0.3574	0.3496	0.3388	0.3249
-30.00	0.3466	0.3450	0.3404	0.3326	0.3218	0.3079
-35.00	0.3264	0.3249	0.3202	0.3125	0.3017	0.2877
-40.00	0.3032	0.3017	0.2970	0.2893	0.2785	0.2645
-45.00	0.2769	0.2754	0.2707	0.2630	0.2521	0.2382
-50.00	0.2475	0.2460	0.2413	0.2336	0.2227	0.2088
-55.00	0.2150	0.2135	0.2088	0.2011	0.1902	0.1763

Y	X					
	30.000	35.000	40.000	45.000	50.000	55.000
0.0000	0.3466	0.3264	0.3032	0.2769	0.2475	0.2150
-5.00	0.3450	0.3249	0.3017	0.2754	0.2460	0.2135
-10.00	0.3404	0.3202	0.2970	0.2707	0.2413	0.2088
-15.00	0.3326	0.3125	0.2893	0.2630	0.2336	0.2011
-20.00	0.3218	0.3017	0.2785	0.2521	0.2227	0.1902
-25.00	0.3079	0.2877	0.2645	0.2382	0.2088	0.1763
-30.00	0.2908	0.2707	0.2475	0.2212	0.1918	0.1593
-35.00	0.2707	0.2506	0.2274	0.2011	0.1717	0.1392
-40.00	0.2475	0.2274	0.2042	0.1779	0.1485	0.1160
-45.00	0.2212	0.2011	0.1779	0.1515	0.1221	0.0896
-50.00	0.1918	0.1717	0.1485	0.1221	0.0927	0.0602
-55.00	0.1593	0.1392	0.1160	0.0896	0.0602	0.0277

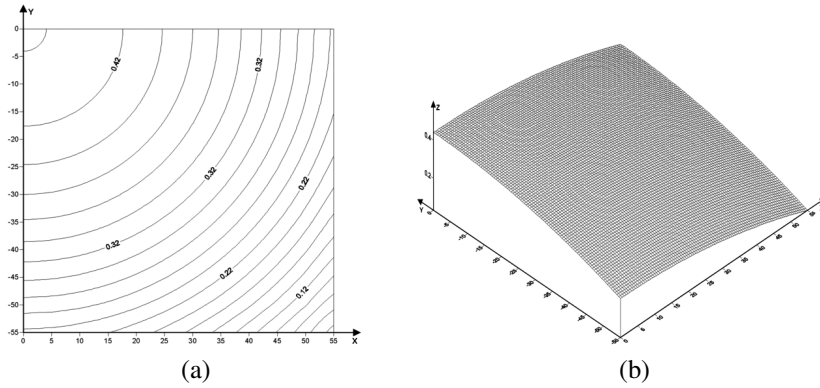


Figure 5: Velocity isolines a) and surface b) at a temperature of 1398 [K]

Table2. Copper melt’s flow velocity profiles at temperature of 1398 [K]

Y	X					
	0.0000	5.0000	10.000	15.000	20.000	25.000
0.0000	0.4412	0.4395	0.4344	0.4259	0.4140	0.3987
-5.00	0.4395	0.4378	0.4327	0.4242	0.4123	0.3970
-10.00	0.4344	0.4327	0.4276	0.4191	0.4072	0.3919
-15.00	0.4259	0.4242	0.4191	0.4106	0.3987	0.3835
-20.00	0.4140	0.4123	0.4072	0.3987	0.3869	0.3716
-25.00	0.3987	0.3970	0.3919	0.3835	0.3716	0.3563
-30.00	0.3801	0.3784	0.3733	0.3648	0.3529	0.3376
-35.00	0.3580	0.3563	0.3512	0.3427	0.3308	0.3156
-40.00	0.3325	0.3308	0.3258	0.3173	0.3054	0.2901
-45.00	0.3037	0.3020	0.2969	0.2884	0.2765	0.2613
-50.00	0.2714	0.2697	0.2646	0.2562	0.2443	0.2290
-55.00	0.2358	0.2341	0.2290	0.2205	0.2086	0.1934

Y	X					
	30.000	35.000	40.000	45.000	50.000	55.000
0.0000	0.3801	0.3580	0.3325	0.3037	0.2714	0.2358
-5.00	0.3784	0.3563	0.3308	0.3020	0.2697	0.2341
-10.00	0.3733	0.3512	0.3258	0.2969	0.2646	0.2290
-15.00	0.3648	0.3427	0.3173	0.2884	0.2562	0.2205
-20.00	0.3529	0.3308	0.3054	0.2765	0.2443	0.2086
-25.00	0.3376	0.3156	0.2901	0.2613	0.2290	0.1934
-30.00	0.3190	0.2969	0.2714	0.2426	0.2103	0.1747
-35.00	0.2969	0.2748	0.2494	0.2205	0.1883	0.1526
-40.00	0.2714	0.2494	0.2239	0.1951	0.1628	0.1272
-45.00	0.2426	0.2205	0.1951	0.1662	0.1340	0.0983
-50.00	0.2103	0.1883	0.1628	0.1340	0.1017	0.0661
-55.00	0.1747	0.1526	0.1272	0.0983	0.0661	0.0304

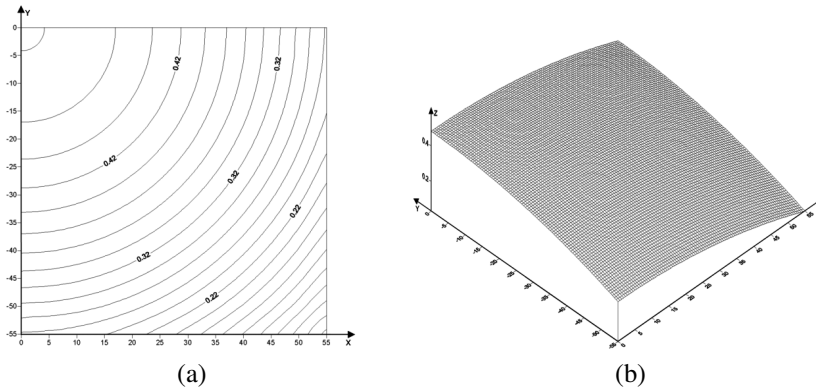


Figure 6: Velocity isolines a) and surface b) at a temperature of 1438 [K]

Table 3. Copper melt's flow velocity profiles at temperature of 1438 [K]

Y	X					
	0.0000	5.0000	10.000	15.000	20.000	25.000
0.0000	0.4814	0.4795	0.4740	0.4647	0.4517	0.4351
-5.00	0.4795	0.4777	0.4721	0.4629	0.4499	0.4332
-10.00	0.4740	0.4721	0.4666	0.4573	0.4443	0.4277
-15.00	0.4647	0.4629	0.4573	0.4480	0.4351	0.4184
-20.00	0.4517	0.4499	0.4443	0.4351	0.4221	0.4054
-25.00	0.4351	0.4332	0.4277	0.4184	0.4054	0.3888
-30.00	0.4147	0.4128	0.4073	0.3980	0.3851	0.3684
-35.00	0.3906	0.3888	0.3832	0.3740	0.3610	0.3443
-40.00	0.3628	0.3610	0.3554	0.3462	0.3332	0.3165
-45.00	0.3314	0.3295	0.3240	0.3147	0.3017	0.2851
-50.00	0.2962	0.2943	0.2888	0.2795	0.2665	0.2499
-55.00	0.2573	0.2554	0.2499	0.2406	0.2276	0.2110

Y	X					
	30.000	35.000	40.000	45.000	50.000	55.000
0.0000	0.4147	0.3906	0.3628	0.3314	0.2962	0.2573
-5.00	0.4128	0.3888	0.3610	0.3295	0.2943	0.2554
-10.00	0.4073	0.3832	0.3554	0.3240	0.2888	0.2499
-15.00	0.3980	0.3740	0.3462	0.3147	0.2795	0.2406
-20.00	0.3851	0.3610	0.3332	0.3017	0.2665	0.2276
-25.00	0.3684	0.3443	0.3165	0.2851	0.2499	0.2110
-30.00	0.3480	0.3240	0.2962	0.2647	0.2295	0.1906
-35.00	0.3240	0.2999	0.2721	0.2406	0.2054	0.1665
-40.00	0.2962	0.2721	0.2443	0.2128	0.1776	0.1388
-45.00	0.2647	0.2406	0.2128	0.1813	0.1462	0.1073
-50.00	0.2295	0.2054	0.1776	0.1462	0.1110	0.0721
-55.00	0.1906	0.1665	0.1388	0.1073	0.0721	0.0332

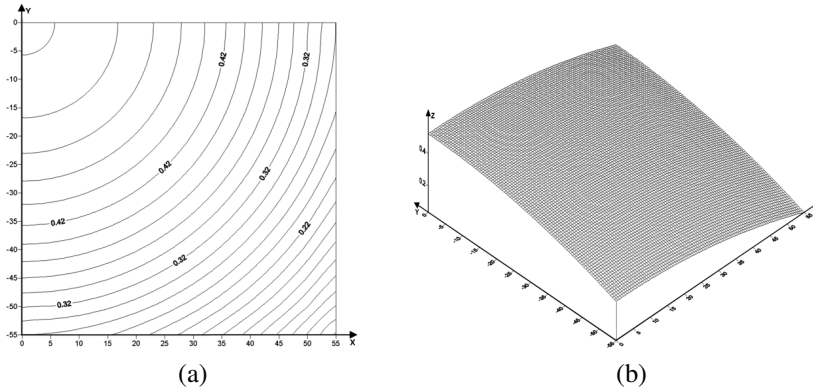


Figure 7: Velocity isolines a) and surface b) at a temperature of 1478 [K]

Table 4. Copper melt's flow velocity profiles at temperature of 1478 [K]

Y	X					
	0.0000	5.0000	10.000	15.000	20.000	25.000
0.0000	0.5227	0.5207	0.5147	0.5046	0.4906	0.4725
-5.00	0.5207	0.5187	0.5127	0.5026	0.4886	0.4705
-10.00	0.5147	0.5127	0.5067	0.4966	0.4825	0.4644
-15.00	0.5046	0.5026	0.4966	0.4865	0.4725	0.4544
-20.00	0.4906	0.4886	0.4825	0.4725	0.4584	0.4403
-25.00	0.4725	0.4705	0.4644	0.4544	0.4403	0.4222
-30.00	0.4503	0.4483	0.4423	0.4322	0.4182	0.4001
-35.00	0.4242	0.4222	0.4161	0.4061	0.3920	0.3739
-40.00	0.3940	0.3920	0.3860	0.3795	0.3618	0.3437
-45.00	0.3598	0.3578	0.3518	0.3417	0.3277	0.3096
-50.00	0.3216	0.3196	0.3136	0.3035	0.2894	0.2713
-55.00	0.2794	0.2774	0.2713	0.2613	0.2472	0.2291

Y	X					
	30.000	35.000	40.000	45.000	50.000	55.000
0.0000	0.4503	0.4242	0.3940	0.3598	0.3216	0.2794
-5.00	0.4483	0.4222	0.3920	0.3578	0.3196	0.2774
-10.00	0.4423	0.4161	0.3860	0.3518	0.3136	0.2713
-15.00	0.4322	0.4061	0.3759	0.3417	0.3035	0.2613
-20.00	0.4182	0.3920	0.3618	0.3277	0.2894	0.2472
-25.00	0.4001	0.3739	0.3437	0.3096	0.2713	0.2291
-30.00	0.3779	0.3518	0.3216	0.2874	0.2492	0.2070
-35.00	0.3518	0.3256	0.2955	0.2613	0.2231	0.1808
-40.00	0.3216	0.2955	0.2653	0.2311	0.1929	0.1507
-45.00	0.2874	0.2613	0.2311	0.1969	0.1587	0.1165
-50.00	0.2492	0.2231	0.1929	0.1587	0.1205	0.0783
-55.00	0.2070	0.1808	0.1507	0.1165	0.0783	0.0360

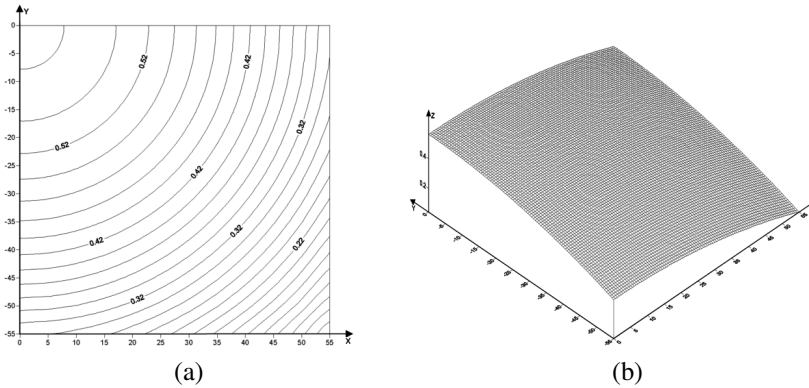


Figure 8: Velocity isolines a) and surface b) at a temperature of 1518 [K]

Table 5. Copper melt’s flow velocity profiles at temperature of 1518 [K]

Y	X					
	0.0000	5.0000	10.000	15.000	20.000	25.000
0.0000	0.5654	0.5207	0.5633	0.5567	0.5306	0.5111
-5.00	0.5633	0.5187	0.5611	0.5546	0.5285	0.5089
-10.00	0.5567	0.5127	0.5546	0.5480	0.5219	0.5024
-15.00	0.5459	0.5026	0.5437	0.5372	0.5111	0.4915
-20.00	0.5306	0.4886	0.5285	0.5219	0.4958	0.4762
-25.00	0.5111	0.4705	0.5089	0.5024	0.4762	0.4567
-30.00	0.4871	0.4483	0.4850	0.4784	0.4523	0.4327
-35.00	0.4588	0.4222	0.4567	0.4501	0.4240	0.4045
-40.00	0.4262	0.3920	0.4240	0.4175	0.3914	0.3718
-45.00	0.3892	0.3578	0.3871	0.3805	0.3544	0.3348
-50.00	0.3479	0.3196	0.3457	0.3392	0.3131	0.2935
-55.00	0.3022	0.2774	0.3000	0.2935	0.2674	0.2478

Y	X					
	30.000	35.000	40.000	45.000	50.000	55.000
0.0000	0.4871	0.4588	0.4262	0.3892	0.3479	0.3022
-5.00	0.4850	0.4567	0.4240	0.3871	0.3457	0.3000
-10.00	0.4784	0.4501	0.4175	0.3805	0.3392	0.2935
-15.00	0.4675	0.4393	0.4066	0.3697	0.3283	0.2826
-20.00	0.4523	0.4240	0.3914	0.3544	0.3131	0.2674
-25.00	0.4327	0.4045	0.3718	0.3348	0.2935	0.2478
-30.00	0.4088	0.3805	0.3479	0.3109	0.2696	0.2239
-35.00	0.3805	0.3522	0.3196	0.2826	0.2413	0.1956
-40.00	0.3479	0.3196	0.2870	0.2500	0.2087	0.1630
-45.00	0.3109	0.2826	0.2500	0.2130	0.1717	0.1260
-50.00	0.2696	0.2413	0.2087	0.1717	0.1304	0.0847
-55.00	0.2239	0.1956	0.1630	0.1260	0.0847	0.0390

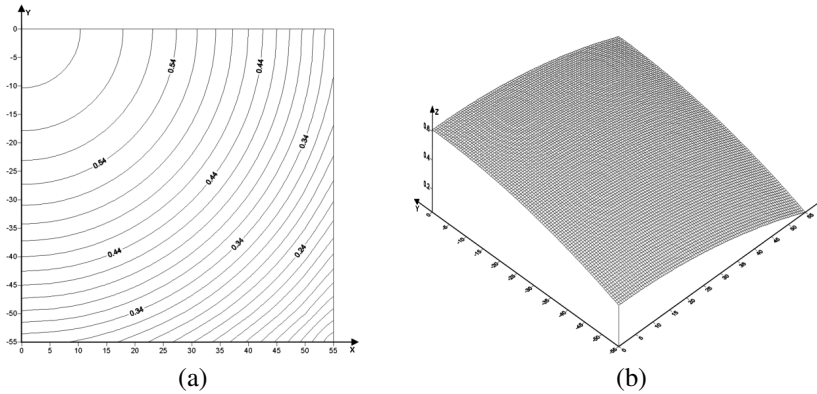


Figure 9: Velocity isolines a) and surface b) at a temperature of 1558 [K]

Table 6. Copper melt’s flow velocity profiles at temperature of 1558 [K]

Y	X					
	0.0000	5.0000	10.000	15.000	20.000	25.000
0.0000	0.6101	0.6078	0.6007	0.5890	0.5726	0.5514
-5.00	0.6078	0.6054	0.5984	0.5867	0.5702	0.5491
-10.00	0.6007	0.5984	0.5913	0.5796	0.5632	0.5421
-15.00	0.5890	0.5867	0.5796	0.5679	0.5514	0.5303
-20.00	0.5726	0.5702	0.5632	0.5514	0.5350	0.5139
-25.00	0.5514	0.5491	0.5421	0.5303	0.5139	0.4928
-30.00	0.5256	0.5233	0.5162	0.5045	0.4881	0.4669
-35.00	0.4951	0.4928	0.4857	0.4740	0.4575	0.4364
-40.00	0.4599	0.4575	0.4505	0.4388	0.4223	0.4012
-45.00	0.4200	0.4176	0.4106	0.3989	0.3824	0.3613
-50.00	0.3754	0.3730	0.3660	0.3543	0.3378	0.3167
-55.00	0.3261	0.3237	0.3167	0.3050	0.2885	0.2674

Y	X					
	30.000	35.000	40.000	45.000	50.000	55.000
0.0000	0.5256	0.4951	0.4599	0.4200	0.3754	0.3261
-5.00	0.5233	0.4928	0.4575	0.4176	0.3730	0.3237
-10.00	0.5162	0.4857	0.4505	0.4106	0.3660	0.3167
-15.00	0.5045	0.4740	0.4388	0.3989	0.3543	0.3050
-20.00	0.4881	0.4575	0.4223	0.3824	0.3378	0.2885
-25.00	0.4669	0.4364	0.4012	0.3613	0.3167	0.2674
-30.00	0.4411	0.4106	0.3754	0.3355	0.2909	0.2416
-35.00	0.4106	0.3801	0.3449	0.3050	0.2604	0.2111
-40.00	0.3754	0.3449	0.3097	0.2698	0.2252	0.1759
-45.00	0.3355	0.3050	0.2698	0.2299	0.1853	0.1360
-50.00	0.2909	0.2604	0.2252	0.1853	0.1407	0.0914
-55.00	0.2416	0.2111	0.1759	0.1360	0.0914	0.0421

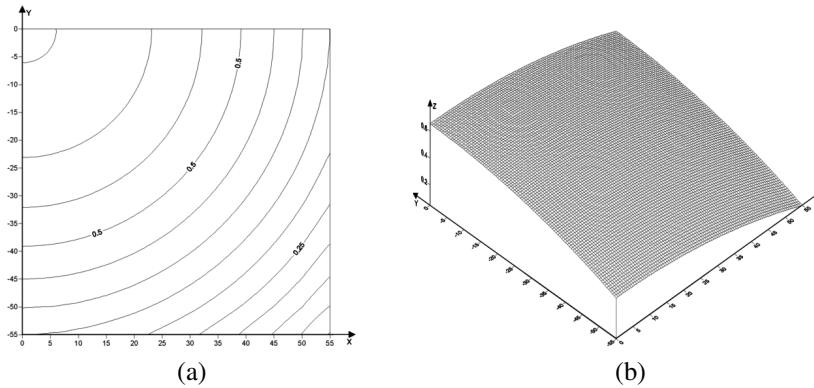


Figure 10: Velocity isolines a) and surface b) at a temperature of 1598 [K]

Table 7. Copper melt’s flow velocity profiles at temperature of 1598 [K]

Y	X					
	0.0000	5.0000	10.000	15.000	20.000	25.000
0.0000	0.6539	0.6513	0.6438	0.6312	0.6136	0.5910
-5.00	0.6513	0.6488	0.6413	0.6287	0.6111	0.5884
-10.00	0.6438	0.6413	0.6337	0.6211	0.6035	0.5809
-15.00	0.6312	0.6287	0.6211	0.6086	0.5910	0.5683
-20.00	0.6136	0.6111	0.6035	0.5910	0.5734	0.5507
-25.00	0.5910	0.5884	0.5809	0.5683	0.5507	0.5281
-30.00	0.5633	0.5608	0.5532	0.5406	0.5230	0.5004
-35.00	0.5306	0.5281	0.5205	0.5079	0.4903	0.4677
-40.00	0.4929	0.4903	0.4828	0.4702	0.4526	0.4300
-45.00	0.4501	0.4476	0.4400	0.4274	0.4098	0.3872
-50.00	0.4023	0.3998	0.3922	0.3797	0.3620	0.3394
-55.00	0.3495	0.3469	0.3394	0.3268	0.3092	0.2866

Y	X					
	30.000	35.000	40.000	45.000	50.000	55.000
0.0000	0.5633	0.5306	0.4929	0.4501	0.4023	0.3495
-5.00	0.5608	0.5281	0.4903	0.4476	0.3998	0.3469
-10.00	0.5532	0.5205	0.4828	0.4400	0.3922	0.3394
-15.00	0.5406	0.5079	0.4702	0.4274	0.3797	0.3268
-20.00	0.5230	0.4903	0.4526	0.4098	0.3620	0.3092
-25.00	0.5004	0.4677	0.4300	0.3872	0.3394	0.2866
-30.00	0.4727	0.4400	0.4023	0.3595	0.3117	0.2589
-35.00	0.4400	0.4073	0.3696	0.3268	0.2790	0.2262
-40.00	0.4023	0.3696	0.3319	0.2891	0.2413	0.1885
-45.00	0.3595	0.3268	0.2891	0.2463	0.1985	0.1457
-50.00	0.3117	0.2790	0.2413	0.1985	0.1507	0.0979
-55.00	0.2589	0.2262	0.1885	0.1457	0.0979	0.0451

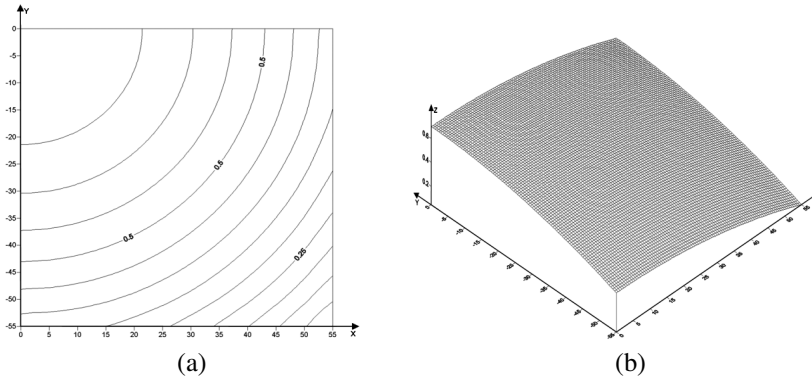


Figure 11: Velocity isolines a) and surface b) at a temperature of 1638 [K]

Table 8. Copper melt’s flow velocity profiles at temperature of 1638 [K]

Y	X					
	0.0000	5.0000	10.000	15.000	20.000	25.000
0.0000	0.6994	0.6967	0.6887	0.6752	0.6564	0.6321
-5.00	0.6967	0.6940	0.6860	0.6725	0.6537	0.6295
-10.00	0.6887	0.6860	0.6779	0.6644	0.6456	0.6214
-15.00	0.6752	0.6725	0.6644	0.6510	0.6321	0.6079
-20.00	0.6564	0.6537	0.6456	0.6321	0.6133	0.5891
-25.00	0.6321	0.6295	0.6214	0.6079	0.5891	0.5649
-30.00	0.6025	0.5999	0.5918	0.5783	0.5595	0.5353
-35.00	0.5676	0.5649	0.5568	0.5433	0.5245	0.5003
-40.00	0.5272	0.5245	0.5164	0.5030	0.4841	0.4599
-45.00	0.4815	0.4788	0.4707	0.4572	0.4384	0.4142
-50.00	0.4303	0.4276	0.4196	0.4061	0.3873	0.3631
-55.00	0.3738	0.3711	0.3631	0.3496	0.3308	0.3065

Y	X					
	30.000	35.000	40.000	45.000	50.000	55.000
0.0000	0.6025	0.5676	0.5272	0.4815	0.4303	0.3738
-5.00	0.5999	0.5649	0.5245	0.4788	0.4276	0.3711
-10.00	0.5918	0.5568	0.5164	0.4707	0.4196	0.3631
-15.00	0.5783	0.5433	0.5030	0.4572	0.4061	0.3496
-20.00	0.5595	0.5245	0.4841	0.4384	0.3873	0.3308
-25.00	0.5353	0.5003	0.4599	0.4142	0.3631	0.3065
-30.00	0.5057	0.4707	0.4303	0.3846	0.3335	0.2769
-35.00	0.4707	0.4357	0.3953	0.3496	0.2985	0.2420
-40.00	0.4303	0.3953	0.3550	0.3092	0.2581	0.2016
-45.00	0.3846	0.3496	0.3092	0.2635	0.2124	0.1559
-50.00	0.3335	0.2985	0.2581	0.2124	0.1612	0.1047
-55.00	0.2769	0.2420	0.2016	0.1559	0.1047	0.0482

Proposed method can be applied to calculate the copper melt movement during bottling from converters, from anode ovens, as well as in a continuous casting and rolling line in the copper wire rod production. It is noteworthy that this temperature is close to optimum temperature for pouring copper at the Joint Venture “Kazkat” in Zhezkazgan.

Thus, the theoretical determined optimum flow temperature of copper melt is consistent with the practical one, being in the optimum 1423–1558 [K] interval, which is close to the temperatures of real melt flow in industrial conditions.

5. Conclusion

The paper presents well converging numerical schemes, using the attempts made to regularize initial systems of differential equations of an incompressible liquid. Lack of the time derivative from the pressure function in the initial system makes it non-evolutionary. This fact was considered as the main one and the regularization ways were proposed to eliminate this “defect”. There were built various $\rho^{N,\varepsilon} \rightarrow \rho^\varepsilon$ -approximations, with a small parameter, introduced into the equation and the time derivative from pressure with a series of terms of the desired functions. However, these approaches proved to be effective only for theoretical justification of the difference schemes convergence. Since the numerical solutions are approximate, it is necessary to substantiate the influence of terms introduced during regularization, which is sometimes difficult. In the paper the authors used Rothe method to construct a difference melt model.

The study of convergence velocity of approximating problem related to the solutions of the original hydrodynamics problem allowed to develop an algorithm for numerical integration of hydrodynamics equations, which allows predicting the technological parameters of metal melts pouring. The validity and reliability of theoretical studies have been confirmed by comparing the results with the parameters of the flow of copper melt in the technological equipment of Southwier-2000 line. The distribution of melt flow velocities in technological equipment has been constructed on the basis of numerical experiments. The theoretically determined optimum flow temperature of copper melt is consistent with the practical one, being in the optimum 1423–1558 [K] interval, which is close to the temperatures of real melt flow in industrial conditions.

References

- [1] R. LAKSHMINARAYANA, K. DADZIE, R. OCONE, M. BORG, and J. REESE: Recasting Navier–Stokes equations. *Journal of Physics Communications*, **3**(10), (2019), 13–18, DOI: [10.1088/2399-6528/ab4b86](https://doi.org/10.1088/2399-6528/ab4b86).

- [2] S.SH. KAZHIKENOVA, S.N. SHALTAQOV, D. BELOMESTNY, and G.S. SHAIHOVA: Finite difference method implementation for Numerical integration hydrodynamic equations melts. *Eurasian Physical Technical Journal*, **17**(33), (2020), 50–56.
- [3] C. BARDOS: A basic example of non linear equations: The Navier–Stokes equations. *Mathematics: Concepts and Foundations*, III (2002), <http://www.eolss.net/sample-chapters/c02/e6-01-06-02.pdf>.
- [4] J. XU and W. YU: Reduced Navier–Stokes equations with streamwise viscous diffusion and heat conduction terms. *AIAA Pap.*, **1441** (1990), 1–6, DOI: [10.2514/6.1990-1441](https://doi.org/10.2514/6.1990-1441).
- [5] Y. SEOKWAN and K. DOCHAN: Three-dimensional incompressible Navier–Stokes solver using lower-upper symmetric Gauss–Seidel algorithm. *AIAA Journal*, **29**(6), (1991), 874–875, DOI: [10.2514/3.10671](https://doi.org/10.2514/3.10671).
- [6] P.M. GRESHO: Incompressible fluid dynamics: some fundamental formulation issues. *Annual Review of Fluid Mechanics*, **23**, (1991), 413–453, DOI: [10.1146/annurev.fl.23.010191.002213](https://doi.org/10.1146/annurev.fl.23.010191.002213).
- [7] S.E. ROGERS, K. DOCHAN, and K. CETIN: Steady and unsteady solutions of the incompressible Navier–Stokes equations. *AIAA Journal*, **29**(4), (1991), 603–610, DOI: [10.2514/3.10627](https://doi.org/10.2514/3.10627).
- [8] S. MASAYOSHI, T. HIROSHI, S. NOBUYUKI, and N. HIDETOSHI: Numerical simulation of three-dimensional viscous flows using the vector potential method. *JSME International Journal*, **34**(2), (1991), 109–114, DOI: [10.1299/jsmeb1988.34.2_109](https://doi.org/10.1299/jsmeb1988.34.2_109).
- [9] E. SCIUBBA: A variational derivation of the Navier–Stokes equations based on the exergy destruction of the flow. *Journal of Mathematical and Physical Sciences*, **25**(1), (1991), 61–68.
- [10] A. BOUZIANI and R. MECHRI: The Rothe’s method to a parabolic integrodifferential equation with a nonclassical boundary conditions. *International Journal of Stochastic Analysis*, Article ID 519684, (2010), DOI: [10.1155/2010/519684](https://doi.org/10.1155/2010/519684).
- [11] N. MERAZGA and A. BOUZIANI: Rothe time-discretization method for a nonlocal problem arising in thermoelasticity. *Journal of Applied Mathematics and Stochastic Analysis*, **2005**(1), (2005), 13–28, DOI: [10.1080/00036818908839869](https://doi.org/10.1080/00036818908839869).

-
- [12] T.A. BARANNYK, A.F. BARANNYK, and I.I. YURYK: Exact solutions of the nonlinear equation. *Ukrains'kyi Matematychnyi Zhurnal*, **69**(9), (2017), 1180–1186, [http://umj.imath.\[K\]iev.ua/index.php/umj/article/view/1768](http://umj.imath.[K]iev.ua/index.php/umj/article/view/1768).
- [13] N.B. ISKAKOVA, A.T. ASSANOVA, and E.A. BAKIROVA: Numerical method for the solution of linear boundary-value problem for integrodifferential equations based on spline approximations. *Ukrains'kyi Matematychnyi Zhurnal*, **71**(9), (2019), 1176–91, [http://umj.imath.\[K\]iev.ua/index.php/umj/article/view/1508](http://umj.imath.[K]iev.ua/index.php/umj/article/view/1508).
- [14] S.L. SKOROKHODOV and N.P. KUZMINA: Analytical-numerical method for solving an Orr-Sommerfeld type problem for analysis of instability of ocean currents. *Zh. Vychisl. Mat. Mat. Fiz.*, **58**(6), (2018), 1022–1039, DOI: [10.7868/S0044466918060133](https://doi.org/10.7868/S0044466918060133).